Journal of Biological Physics (2022) 48:253–272
https://doi.org/10.1007/s10867-022-09607-x

ORIGINAL PAPER

"Flexible hinge" dynamics in mismatched DNA revealed by fluorescence correlation spectroscopy

Timour B. Ten[1] · Viktoriya Zvoda[1] · Manas K. Sarangi[1,2] · Serguei V. Kuznetsov[1] · Anjum Ansari[1]

Received: 31 October 2021 / Accepted: 22 March 2022 / Published online: 22 April 2022

Abstract

Altered unwinding/bending fluctuations at DNA lesion sites are implicated as plausible mechanisms for damage sensing by DNA-repair proteins. These dynamics are expected to occur on similar timescales as one-dimensional (1D) diffusion of proteins on DNA if effective in stalling these proteins as they scan DNA. We examined the flexibility and dynamics of DNA oligomers containing 3 base pair (bp) mismatched sites specifically recognized in vitro by nucleotide excision repair protein Rad4 (yeast ortholog of mammalian XPC). A previous Forster resonance energy transfer (FRET) study mapped DNA conformational distributions with cytosine analog FRET pair primarily sensitive to DNA twisting/unwinding deformations (Chakraborty et al. Nucleic Acids Res. 46: 1240–1255 (2018)). These studies revealed B-DNA conformations for nonspecific (matched) constructs but significant unwinding for mismatched constructs specifically recognized by Rad4, even in the absence of Rad4. The timescales of these unwinding fluctuations, however, remained elusive. Here, we labeled DNA with Atto550/Atto647N FRET dyes suitable for fluorescence correlation spectroscopy (FCS). With these probes, we detected higher FRET in specific, mismatched DNA compared with matched DNA, reaffirming unwinding/bending deformations in mismatched DNA. FCS unveiled the dynamics of these spontaneous deformations at ~ 300 μs with no fluctuations detected for matched DNA within the ~ 600 ns–10 ms FCS time window. These studies are the first to visualize anomalous unwinding/bending fluctuations in mismatched DNA on timescales that overlap with the < 500 μs "stepping" times of repair proteins on DNA. Such "flexible hinge" dynamics at lesion sites could arrest a diffusing protein to facilitate damage interrogation and recognition.

Keywords DNA unwinding/bending dynamics · Spontaneous fluctuations · Mismatched DNA dynamics · DNA damage recognition · Conformational energy landscape

This article belongs to the Topical Collection: The Revolutionary Impact of Landscapes in Biology
Guest Editors: Robert Austin, Shyamsunder Erramilli, Sonya Bahar

✉ Anjum Ansari
ansari@uic.edu

[1] Department of Physics (M/C 273), University of Illinois at Chicago, Chicago, IL 60607, USA

[2] Present Address: Department of Physics, Indian Institute of Technology, Patna 801103, India

1 Introduction

How DNA damage repair proteins search for and identify damaged sites buried in a sea of undamaged genomic DNA remains a puzzle. These proteins need to rapidly scan DNA and yet slow down at potential "trouble spots" to interrogate and recognize damage to initiate repair. This is particularly challenging in the mismatch-repair (MMR) and nucleotide excision repair (NER) pathways where the damage sensing proteins exhibit broad specificity for a wide variety of structurally dissimilar lesions. These lesions nonetheless share a common theme in that they locally destabilize DNA, and damage recognition in both MMR and NER relies almost entirely on "indirect readout" where the roving proteins likely sense differences in local DNA deformability to discriminate damaged from undamaged sites [1–3]. This initial recognition is dictated entirely by thermal fluctuations and conformational adaptation; however, the conformational dynamics in proteins and DNA that enable recognition remain poorly characterized [4].

The one-dimensional (1D) diffusion constants of several damage sensing proteins diffusing on largely undamaged DNA have been measured to be in the range ~ 0.0001–1 $\mu m^2/s$ [5–12] that translate into residence times per base pair (bp) of ~ 0.05–500 μs, assuming a stepping distance of ~ 1 bp. Efficient interrogation must occur on similar timescales before the protein diffuses away. Such interrogation dynamics were recently unveiled for the NER damage sensing protein Rad4 (yeast ortholog of the mammalian XPC protein) and another site-specific DNA bending protein, the architectural nucleoid-associated prokaryotic protein integration host factor (IHF), using microseconds-resolved laser temperature-jump (T-jump) perturbation approach [13–15]. These studies provided support for the proposed mechanism for the "search/stability" paradox in which proteins, while scanning DNA, intermittently switch from a rapidly diffusing "search" mode to a slower "interrogation" mode [16–20]. However, what role intrinsic DNA fluctuations play in inducing protein conformational changes and ensnaring damage sensing proteins at potential damaged sites remains an outstanding question. Structures of repair proteins with damaged DNA reveal severely disrupted DNA [1, 3, 21] and implicate intrinsic DNA deformability and altered "flexible hinge" dynamics at lesion sites in facilitating damage sensing [1, 2, 22–25]. Visualizing DNA conformational dynamics that could impact 1D diffusion of repair proteins in the vicinity of the lesion sites has proven to be challenging.

Here, we examined the conformational dynamics of short DNA oligomers harboring a 3 base pair (bp) mismatch. The choice of these DNA substrates was motivated by previous structural and dynamics studies of damage recognition mechanism by Rad4/XPC [3, 14, 26]. Rad4/XPC recognizes structurally diverse, bulky, helix-destabilizing lesions induced by UV light or genotoxins and recruits downstream proteins that verify and excise the lesion-containing strand followed by repair [27–32]. In vitro Rad4 can bind 2- or 3-bp mismatches with affinities similar to that of *bonafide* NER substrates [3, 25, 26], thus providing us with suitable model systems for biophysical studies of DNA damage recognition mechanisms.

Structural studies showed that Rad4, when bound to NER substrates or to model lesions, unwinds and bends DNA at the lesion sites, flips out two damage-containing nucleotide pairs from both strands, and inserts a β-hairpin to stabilize this recognition complex [3, 33]. Notably, in this so-called "open" structure, Rad4 makes no direct contact with the damaged nucleotides, which are flipped away from the protein; instead, it interacts exclusively with the nucleotides flipped out from the complementary, undamaged strand. Such an indirect mode of recognition revealed how Rad4 binds to a diverse set of lesions [3,

34]. Remarkably, this Rad4 interaction is not exclusive to damaged DNA; when covalently tethered to undamaged DNA—to minimize heterogeneous binding inherent in nonspecific complexes—Rad4 flips out nucleotides to form the same "open" structure [26, 35]. These results pointed to a "kinetic gating" mechanism whereby lesion selectivity comes from differences in kinetics rather than in the Rad4-bound stable structures, e.g., a kinetic competition between the ability of Rad4 to flip nucleotides at a given site versus diffusing away [26]. Laser T-jump studies on Rad4 bound to DNA containing 2- or 3-bp mismatches revealed nucleotide-flipping kinetics on timescales of ~ 5–10 ms [14, 26]. Kinetics of nucleotide flipping from within undamaged DNA have not been measured. However, free energy calculations indicate much higher energy barrier (> 5 kcal/mol) for extruding nucleotides from undamaged versus damaged DNA [22], suggesting that Rad4-facilitated flipping of nucleotides from within undamaged DNA should be much slower than for damaged DNA. These differences could explain how a freely diffusing protein would preferentially flip nucleotides from within helix-destabilizing lesions and avoid inefficient flipping from within every undamaged site as it scanned DNA.

The rates at which Rad4 flips out nucleotides from within damaged versus undamaged site are one facet of the proposed kinetic gating mechanism. The other facet is the "residence" time or "stepping" time of the diffusing protein per base pair site, i.e., the average time the protein sits on one site before jumping or sliding to the next site. Single-molecule imaging studies of Rad4 or XPC diffusing on long stretches of undamaged DNA indicate average residence times per bp site of ~ 1–200 μs [10] and ~ 0.05–10 μs [11], respectively, under ~ 75–150 mM monovalent ionic conditions. The broad distributions in the measured diffusion coefficients are attributed to either the fluctuating conformations of the protein or sequence-dependent changes in local DNA conformations. These residence times per bp site for Rad4 are 25- to 10,000-fold smaller than the T-jump measured nucleotide flipping times in Rad4-bound mismatched DNA complexes. This separation in timescales would suggest inefficient recognition, since the protein would have a high probability of diffusing away before it had sufficient time to form a recognition complex. Indeed, evidence for such inefficient recognition for a substrate only modestly preferred by Rad4/XPC—the cyclobutane pyrimidine dimer (CPD) lesion—was recently obtained from studies of XPC diffusing on CPD-containing DNA [11]. One plausible explanation for how diffusing proteins could get arrested preferentially at damaged sites is if the local DNA structure and/or dynamics at that site were significantly altered compared with undamaged DNA. A growing body of evidence shows enhanced flexibility localized at the mismatched or otherwise damaged sites [1, 36–52]. Much less is known about the extent to which these localized fluctuations affect overall DNA conformations such as unwinding and bending and what the timescales are on which these dynamics occur.

To examine such conformational distortions in 3-bp mismatched DNA specifically recognized by Rad4, we previously used fluorescence lifetime (FLT) studies with cytosine analogs (tC^o and tC_{nitro}) FRET pair placed on either side and in close proximity to the mismatched site [25]. These probes exhibit normal base pairing with guanine with minimal perturbation of DNA structure and stability, making the FRET efficiency (E) between them sensitive to changes in DNA helicity and therefore to unwinding distortions in DNA conformations [14, 53–56]. Furthermore, incorporation of these probes in DNA at the sites shown in Fig. 1 did not significantly impact Rad4 binding affinities for 3-bp mismatched and matched DNA as measured by competition gel-shift assays [14, 25]. With FLT-FRET, we mapped the DNA conformational distributions and unveiled large-amplitude deviations from B-DNA for constructs containing 3-bp CCC/CCC mismatch specifically recognized by Rad4 (Fig. 1). Notably, mismatched DNA alone displayed conformations that resembled

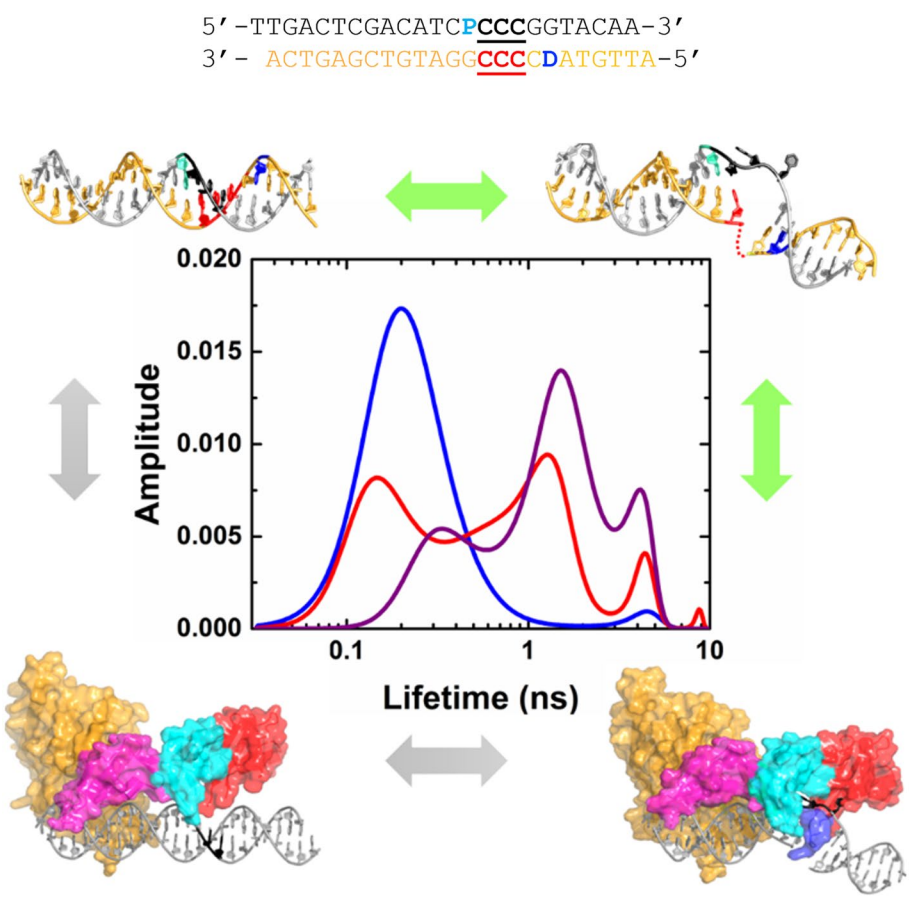

Fig. 1 Fluorescence lifetime studies with tC^o-tC_{nitro}-labeled DNA. (Top) Sequence of DNA constructs with CCC/CCC mismatch and labeled with FRET pair tC^o (D: donor) and tC_{nitro} (P: acceptor). Lifetime distributions on matched DNA (blue) are predominantly single-peaked and represent the ensemble of B-DNA-like conformations. Corresponding distributions on mismatched (CCC/CCC) DNA show multiple components for both free (red) and Rad4-bound DNA (purple). Structures shown are (clockwise from top left): model B-DNA structure; DNA structure in a Rad4-bound specific complex (from PDB code 2QSH); Rad4-bound specific complex structure (PDB code 2QSH); apo-Rad4 structure (PDB code 2QSF) superimposed on the model B-DNA. Figure reproduced from ref. [25], by permission of Oxford University Press

structures in the Rad4-bound specific complex. These studies provided compelling (albeit indirect) evidence for unusual DNA dynamics as a likely feature that Rad4 senses during interrogation. While FLT-FRET studies offered snapshots of accessible conformations in mismatched DNA, alone and with Rad4, the timescales eluded us.

To measure DNA dynamics, we turned to fluorescence correlation spectroscopy (FCS) studies on the CCC/CCC mismatched DNA, but this time labeled with extrinsic, higher quantum yield dyes that are suitable for single-molecule studies. With these probes, we detected changes in FRET between mismatched and matched DNA constructs, consistent with an increase in overall DNA bending in the presence of the mismatch. More importantly, FCS studies on freely diffusing mismatched DNA constructs uncovered ~ 300 μs spontaneous conformational fluctuations that were not observed on matched DNA. To our

knowledge, these are the first direct observations of intrinsic unwinding/bending dynamics in mismatched DNA. Notably, the timescales of these fluctuations overlap with 1D residence times of Rad4/XPC. These observations provide a missing crucial piece in the puzzle of how anomalous fluctuations in damaged DNA could be a mechanism for stalling a diffusing protein and engaging it preferentially at a "faulty" DNA site.

2 Materials and methods

2.1 Preparation and characterization of DNA complexes

27-nucleotide-long DNA oligonucleotides containing the Atto550 and Atto647N fluorescent probes were purchased from Eurofins Genomics with reverse-phase HPLC purification. Annealing to make duplex DNA was done in phosphate-buffered saline (PBS) (10 mM Na_2HPO_4, 2 mM KH_2PO_4, 137 mM NaCl, 2.7 mM KCl, pH 7.4) as described in SI Methods 1.1.

2.2 Picoseconds-resolved fluorescence spectroscopy

Fluorescence decay curves were measured with a PicoMaster fluorescence lifetime instrument (HORIBA-PTI, London, Ontario, Canada) equipped with time-correlated single photon counting (TSCPC) electronics [57]. Further details of the apparatus and data acquisition are in SI Methods 1.2. For all FRET measurements, decay traces were measured for donor-only (DNA_D) duplexes without acceptor as well as donor–acceptor (DNA_DA) duplexes.

2.3 Analysis of the fluorescence decay traces

Decay curves were analyzed as described previously [25], either as a sum of discrete exponentials (DE; SI Methods 1.3) convoluted with the instrument response function (IRF), or using a maximum entropy method (MEM; SI Methods 1.4), in which the effective distribution of log-lifetimes $f(\log\tau)$ was inferred from the decay traces using the program MemExp [58, 59] (available online). The MEM distributions were further analyzed as a sum of Gaussian distributions (SI Methods 1.5). The average FRET efficiency value reported for each sample was computed as $< E >= 1 - \frac{<\tau_{DA}>}{<\tau_D>}$, where $< \tau_D >$ and $< \tau_{DA} >$ are the average lifetimes for donor-only or donor–acceptor labeled samples, respectively, and were computed as described in SI Methods 1.3–1.4. The lifetime and FRET E values reported in the text are from the MEM analysis, unless otherwise noted.

2.4 Fluorescence correlation spectroscopy

The fluorescence correlation spectroscopy (FCS) measurements were carried out on a custom-built apparatus based on an inverted Olympus IX70 microscope. In this setup, a collimated 532-nm laser beam from a diode laser (GCL-050 Laser CrystaLaser) was expanded to 8 mm diameter and then focused through a water immersion objective (Olympus UPLANSApo 60X, NA 1.2) onto the sample, which was sandwiched between a glass cover slip (VWR No.1 coverslip; 24 mm by 30 mm, with thickness 150 ± 20 μm) and a

CoverWell PC8R-0.5 perfusion chamber. The fluorescence was collected by the same objective. The excitation and emission beams were separated by a dichroic mirror (Semrock DI03-R532-T1-25X36) that was installed immediately under the objective turret. The emission beam was focused through the side port of the microscope on a 50-μm pinhole. A second dichroic mirror (640 nm; Semrock FF640-FDI02-T3-25 × 36) installed after the pinhole was used to separate the donor (Atto550) and acceptor (Atto647N) emission beams, each of which were then imaged onto two separate avalanche photodiode detectors (APD, PerkinElmer SPCM-AQR-14-FC) using two 15-cm apochromatic lenses (Newport PAC075AR.14), each placed at a two-focal distance between the pinhole and each of the APDs. Both APDs were connected to a digital correlator (Flex02-01D) and the correlation functions were produced by the Flex software.

Measurements on matched and mismatched DNA were conducted on 10-nM donor-only (DNA_D) and donor–acceptor-labeled (DNA_DA) samples. Correlation traces were collected from each sample (60 μL) for about 5 min, with 5 replicates, for a total acquisition time of 25 min. The correlation traces presented are the average from the 5 repeats and the uncertainties in the data are the standard error of the mean (s.e.m.). Corresponding correlation traces on buffer only samples were obtained each day of the measurement under identical microscope alignment conditions as for the TAMRA or DNA samples and were used to subtract detector "after-pulsing" artifacts from the observed correlation traces, as described in SI Methods 1.6. Calibration of the confocal volume was performed using a reference sample, TAMRA dye, with a known diffusion coefficient $D_{ref} \approx 420\ \mu m^2/s$ [60–62], as described in SI Methods 1.7.

Intensity fluctuations in the donor (D) and acceptor (A) channels are quantified by the auto- (G_{DD} or G_{AA}) or cross- (G_{DA}) correlation functions of the fluorescence fluctuations, defined as:

$$G_{XY}(\tau) = \frac{\langle \delta I_X(t) \delta I_y(t+\tau) \rangle}{\langle I_X(t) \rangle \langle I_Y(t) \rangle} = \frac{\langle I_X(t) I_y(t+\tau) \rangle}{\langle I_X(t) \rangle \langle I_Y(t) \rangle} - 1 \tag{1}$$

where the angle brackets represent a time average over the data accumulation time and $\delta I_{X,Y}(t) = I_{X,Y}(t) - \langle I_{X,Y}(t) \rangle$ is the instantaneous deviation from the average. The correlation curves measured for DNA_D and DNA_DA samples were further analyzed to extract the diffusion coefficients of the diffusing molecules and any conformational relaxation kinetics. We followed the formalism as outlined by Torres and Levitus [63] and described in more detail in SI Methods 1.8. Briefly, the correlation functions on donor–acceptor labeled samples were expected to have contributions from the diffusion of the molecules in and out of the confocal volume, characterized by $G_{diff}(\tau)$, as well as from any conformational fluctuations, characterized by $G_{conf\_XY}(\tau)$, such that

$$G_{XY}(\tau) = G_{conf\_XY}(\tau) G_{diff}(\tau) \tag{2}$$

The contributions of the conformational fluctuations to $G_{DD}(\tau)$ and $G_{AA}(\tau)$ were further parameterized as

$$G_{conf\_DD}(\tau) = 1 + \gamma_{DD} e^{-\tau/\tau_{rel}} \tag{3}$$

$$G_{conf\_AA}(\tau) = 1 + \gamma_{AA} e^{-\tau/\tau_{rel}} \tag{4}$$

where the pre-exponentials γ_{DD} and γ_{AA} depend on the FRET levels and interconversion rates between two distinct conformations of a given molecule and τ_{rel} is the conformational relaxation time constant (see SI Methods 1.8). While this simple formalism assumes only two conformational states, the signal-to-noise in our correlation functions did not merit consideration of additional states.

For each donor–acceptor (DNA_DA) samples, we simultaneously acquired the donor-donor $G_{DD}(\tau)$ and the acceptor-acceptor $G_{AA}(\tau)$ auto-correlation functions from the intensity traces acquired by the donor and acceptor APD's, respectively. The ratio of these two correlation functions (G_{ratio}) directly yields the conformational relaxation component since the diffusion component is identical in both channels and drops out to give:

$$G_{ratio} = \frac{G_{DD}(\tau)}{G_{AA}(\tau)} = \frac{G_{conf\_DD}(\tau)}{G_{conf\_AA}(\tau)} = \frac{1 + \gamma_{DD} e^{-\tau/\tau_{rel}}}{1 + \gamma_{AA} e^{-\tau/\tau_{rel}}} \tag{5}$$

The measured G_{ratio} on DNA_DA samples were fit to the above equation with γ_{AA}, γ_{DD}, and τ_{rel} as free parameters. The donor-only (DNA_D) samples are expected to exhibit only the diffusion component in their correlation functions and were measured as controls. The uncertainties in the reported values of τ_{rel} and the diffusion coefficients represent 95% confidence interval.

3 Results

3.1 DNA conformational distributions measured with fluorescence lifetime studies: an overview

The FRET efficiency (FRET E) between donor and acceptor fluorescent labels placed at two different positions within a duplex DNA can be obtained directly from the lifetimes of the excited donor fluorophore, as $E = 1 - \frac{\tau_{DA}}{\tau_D}$, where τ_{DA} and τ_D are the donor lifetimes in the presence and absence of the acceptor, respectively. The ideal FRET labels for these studies are those for which the fluorescence lifetime of the donor in the absence of the acceptor, i.e., τ_D measured in donor-only labeled DNA constructs (DNA_D), is relatively insensitive to its macromolecular environment [64], with single-exponential decays of the excited state. In the presence of an acceptor to which the donor can transfer energy, as in DNA constructs containing both the donor and the acceptor (DNA_DA), the donor lifetime τ_{DA} is expected to shorten as a result of the FRET, which depends strongly on the relative distance and orientation between the donor and acceptor. Thus, the FRET efficiency and the corresponding τ_{DA} provide a sensitive measure of the DNA conformations harboring the probes. A single conformation with a fixed donor–acceptor distance/orientation is expected to exhibit a single FRET efficiency and hence a single-exponential fluorescence decay trace with a unique τ_{DA}. If the sample consists of multiple conformations (or the dyes adopt different orientations), this heterogeneity is reflected in multiple dye distances/orientations and hence a distribution of FRET efficiencies that yields a multi-exponential decay trace corresponding to a distribution of τ_{DA} lifetimes. The time-resolution of such lifetime instrumentation enables measurements of lifetimes down to < 100 picoseconds (typically limited by the instrument response function of the spectrometer) and enables measurements of the distribution of FRET efficiencies between the probes, even for molecules that may be interconverting on sub-microsecond timescales; such rapidly fluctuating conformations evade detection in single-molecule FRET

studies with total internal reflection fluorescence (TIRF) setups that typically have a time-resolution of tens-of-milliseconds [65, 66].

Previously, we used cytosine analogs tC^o and tC_{nitro} that serve as a FRET pair to detect unwinding deformations in mismatched DNA [25]. However, the tC^o-tC_{nitro} pair is not suitable for the fluorescence correlation spectroscopy measurements we set out to perform, which require higher quantum yield fluorescent probes. To this end, we chose Atto550 (donor) and Atto647N (acceptor) attached to DNA with six carbon linkers at positions shown in Fig. 2. The choice of the labels and the separation of 14 bp between the donor and acceptor probes were based on a previous study with the same design, which reported FRET E of ~ 0.55 for matched DNA with this FRET pair [67]. We obtained FRET E of 0.57 ± 0.02 for matched DNA, in good agreement. The results from the Atto-labeled DNA constructs are described below and summarized in SI Tables S1 and S2.

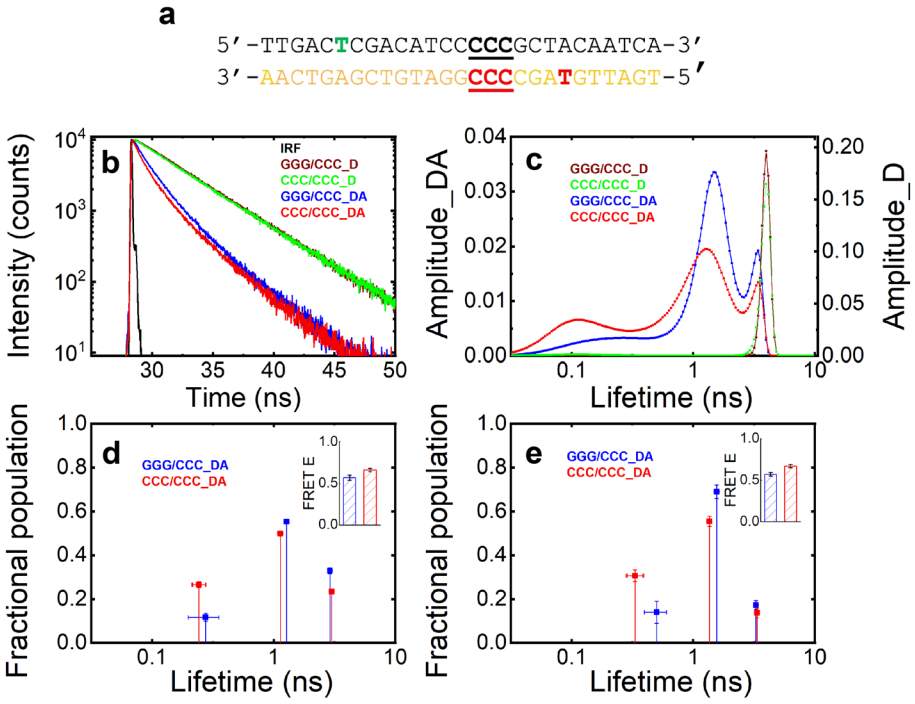

Fig. 2 Fluorescence lifetime measurements on Atto550/Atto647N-labeled DNA constructs. (**a**) Sequence of DNA oligomers used in this study. The red and green thymines indicate the positions where the FRET dyes were attached, with donor (Atto550) in the top strand, and acceptor (Atto647N) in the bottom strand. (**b**) Donor fluorescence intensity decay curves, with excitation at 530 nm, are shown for donor-only labeled samples (GGG/CCC_D: brown; CCC/CCC_D: green) and donor–acceptor labeled samples (GGG/CCC_DA: blue; CCC/CCC_DA: red). The instrument response function (IRF) is shown in black. (**c**) The distribution of lifetimes that best describe the intensity decay profiles, obtained from the maximum entropy method (MEM), are shown. The amplitudes from the MEM analysis, normalized to add up to one, are shown on the left y-axis for DNA_DA and on the right y-axis for DNA_D. (**d**) The fractional population in each of the three components obtained from a discrete exponential analysis of the decay curves are shown versus the lifetime for that component for matched (blue) and mismatched (red) DNA. (**e**) Corresponding average lifetimes and fractional populations obtained from Gaussians fits to the MEM distributions are shown. Three Gaussian components were sufficient to describe the MEM distributions. The insets in (**d**) and (**e**) show average FRET E values for matched (blue) and mismatched (red) DNA. The uncertainties in panels (**d**) and (**e**) are standard error of the mean (s.e.m) from four independent experiments

3.2 Conformational distributions in matched and mismatched DNA

The choice of DNA substrates for this study was motivated by the previous studies that showed specific Rad4 binding to 24-mer DNA oligomers containing 2- or 3-bp mismatches [14, 25, 26, 35]. Competition gel-shift assays showed that Rad4 binds to DNA constructs harboring a CCC/CCC mismatch with a relative binding affinity of ~ 52–60 nM compared with ~ 325–386 nM for the matched counterpart and comparable to ~ 35 nM for a real NER substrate (6–4 photoproduct) [25, 33, 35]. Thus, in this study, we used DNA duplexes with a CCC/CCC mismatched site along with its matched counterpart and examined their conformational distributions, as probed by FRET between the Atto labels (Fig. 2a).

The fluorescence lifetime measurements on donor-only (DNA_D), acceptor-only (DNA_A), and donor–acceptor-labeled (DNA_DA) constructs at 20 °C are shown in Fig. 2 and SI Fig. S1. When analyzed by discrete exponential (DE) analysis, each fluorescence decay trace of the DNA_D and DNA_A constructs could be described in terms of a single-exponential decay with characteristic time constants of 3.93 ± 0.02 ns and 4.43 ± 0.02 ns, respectively, consistent with previously reported lifetime measurements with these probes [68] (SI Methods 1.7; Fig. 2b; SI Fig. S1). In contrast, the DNA_DA constructs exhibited significant deviations from a single-exponential decay, requiring a minimum of three lifetimes for both matched and mismatched constructs (Fig. 2d; SI Fig. S2; SI Tables S1 and S2). Consistent with the DE analyses, the MEM analyses of the decay traces showed single sharp distributions of lifetimes for DNA_D and broader distributions extending from ~ 100 ps to ~ 5 ns for the DNA_DA constructs, with at least three discernible components within the broad distributions (Fig. 2c and SI Fig. S3, S4).

First, we analyzed the average FRET E, which changed from 0.57 ± 0.02 in the matched construct to 0.67 ± 0.02 in the mismatched construct (insets in Fig. 2d, e). Since the local DNA context and the separation of the dyes are unaltered in the two constructs, we conclude that this increase in FRET E in the mismatched DNA reflects a change in the overall helical conformation of the mismatched DNA compared to the matched DNA, and that the Atto labels—as positioned—are sensitive to these conformational changes. These conclusions are consistent with our previous observations of altered DNA conformations in CCC/CCC DNA as detected with the tC^o and tC_{nitro} probes.

Next, we examined the underlying components describing the fluorescence decay curves. To compare the amplitudes and lifetimes of the three components as obtained from the DE analysis (Fig. 2d) with the distribution of lifetimes obtained from MEM (Fig. 2c), we further analyzed the MEM distributions in terms of a sum of Gaussians (SI Fig. S3). The average lifetime (and the corresponding FRET E) of each Gaussian component and the fractional population in each component—computed from the area under the Gaussian curve—are shown in Fig. 2e and summarized in SI Table S2. The reproducibility of the MEM distributions from four independent lifetime measurements on each sample is illustrated in SI Fig. S4; the data presented in Fig. 2c are for one representative from this set. For the most part, lifetime distributions from different measurements on the same sample overlapped, albeit with some variability in the width and height of each underlying peak. Despite this variability, the average lifetimes and fractional populations of the underlying Gaussian components overlap quite well for different measurements, for both matched and mismatched DNA, with only the shortest lifetime component exhibiting significant variability (SI Fig. S4c, d). This variance is attributed to the fact that the shortest lifetime component (~ 240–270 ps) falls close to the instrument response function (IRF) of ~ 140 ps. Notably, the average lifetimes and amplitudes from the MEM/

Gaussian analysis are in excellent agreement with the corresponding results from the DE analysis (compare Fig. 2d, e).

Every DNA_DA construct exhibited some amplitude in a long-lifetime component centered at ~ 3 ns, which is close to, though not overlapping with, the single lifetime component measured for the donor-only DNA_D samples, yielding a FRET E of ~ 0.15–0.17. These results indicate that even the longest lifetime component is not from donor-labeled samples that have a missing or inactive acceptor strand, which should have yielded a component with FRET E of ~ zero. Such "zero-FRET" components are routinely observed in single-molecule FRET measurements and typically discarded as an artifact [69]. To rule out any such contributions from similar artifacts, we performed measurements with increasing concentrations of acceptor strand in our matched DNA samples (SI Fig. S5). Our data showed no change in the fractional amplitudes of the different components even with twofold increase in the acceptor strand concentration, indicating that all components reflect a true FRET state in our samples.

Both the DE and the MEM analyses on the matched construct revealed three components with FRET E values of 0.87 ± 0.03 (14%), 0.61 ± 0.01 (69%), and 0.17 ± 0.01 (17%), respectively. These multiple components reflect either multiple DNA conformations or multiple dye orientations for a fixed conformation that are not averaged out on the timescales of the excited state lifetimes of the donor dye. Our previous measurements with the tC^o and tC_{nitro} probes showed only a predominantly single Gaussian component underlying the lifetime distributions obtained on matched DNA (Fig. 1), with FRET between the probes consistent with what is expected for B-DNA [25]. We therefore attribute the multiple distinct components we observe for the Atto-labeled DNA constructs as arising primarily from different relative orientations of the donor/acceptor dyes. Indeed, previous studies of the photophysical properties of commonly used FRET dyes and measurements of time-resolved polarization anisotropy of these dyes, free and attached to DNA, have shown that Atto550- or Atto647N-labeled DNA duplexes, among other dye-DNA constructs, exhibit two or more anisotropy decay time constants: a fast component consistent with a relatively freely rotating dye and one or more slow components indicative of a dye that is stacked against the DNA [67, 70–72]. This behavior is attributed in part to the +1 charge on the Atto550 and Atto647N labels, which increases their tendency to stick to DNA.

The lifetime distributions of the mismatched constructs also showed three components with corresponding FRET values that are very similar to those seen in the matched constructs (Fig. 2d, e). However, the fractional populations in the three components differed between the two constructs. In particular, the shortest lifetime (high-FRET) component in the mismatched DNA increased ~ twofold compared with the matched counterpart, with a corresponding decrease in the two longer lifetime components. These results suggest that the mismatched DNA by itself can sample bent/unwound conformations not accessed by the matched counterpart, consistent with our conclusions with the tC^o-tC_{nitro} probes.

3.3 DNA conformational dynamics measured with fluorescence correlation spectroscopy: an overview

While the FLT-FRET studies reported above, together with our earlier tC^o-tC_{nitro} studies on similar constructs, provide a snapshot of accessible conformations in mismatched DNA, the timescales eluded us. To measure DNA conformational dynamics, we next turned to fluorescence correlation spectroscopy (FCS) measurements on the Atto-labeled DNA constructs.

The FCS setup is described in Sect. 2. The donor (Atto550) was excited with a 532-nm laser and the fluorescence counts from the donor or the acceptor (Atto647N) were collected by two avalanche photodiode detectors, labeled APD1 and APD2, respectively in Fig. 3.

The measured donor or acceptor fluorescence counts fluctuate either because the number of molecules in the confocal volume fluctuates as the molecules diffuse in or out, or because the molecules undergo a conformational fluctuation that changes the FRET efficiency between the donor and the acceptor. If the diffusion coefficient of the different conformational states of the molecules is assumed to be identical, then the correlation functions can be expressed as the product of a term that represents the kinetics of the conformational fluctuations (G_{conf}) and a term that contains the diffusion contributions (G_{diff}). In practice, the correlation curves also show a large-amplitude sharp decay at short lag times because of detector "after-pulsing" [73, 74]. The after-pulsing component was measured directly from measurements made on buffer only samples and subtracted from the measured correlation functions as described in SI Methods 1.6 and SI Fig. S6, to obtain the corrected (buffer-subtracted) correlation functions that are described below.

3.4 Calibration of the FCS setup

We first established the appropriate range of the excitation laser power for which the measured fluorescence counts scaled linearly with the laser power. These linearity tests were done with a control sample, which was 10 nM free TAMRA dye in water. The fluorescence counts were measured in the donor APD for laser power that ranged from 2–50 μW, measured at the sample position. The plot of fluorescence counts versus laser power is shown in SI Fig. S7, together with the auto-correlation curves shown for several different laser intensity values. The results indicate a linear response until ~50 μW laser power and auto-correlation functions that overlap over that entire laser power range. All subsequent measurements were performed with a laser power of 17.5 μW.

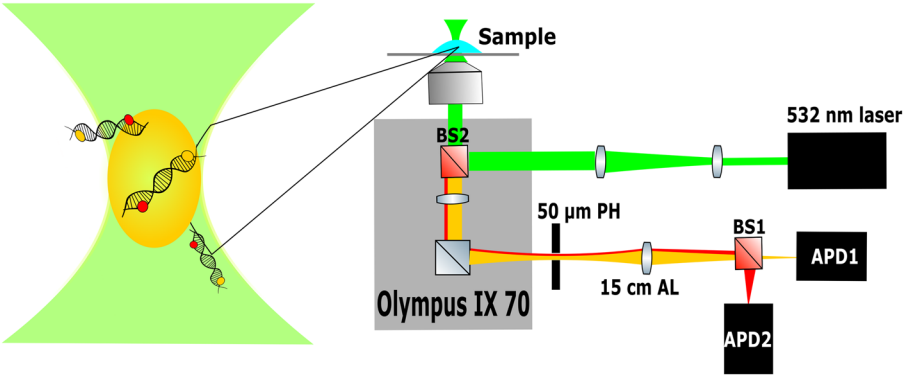

Fig. 3 Schematic of FCS apparatus. A collimated 532-nm laser (excitation) beam is expanded to 8 mm and directed to a dichroic beamsplitter (BS2). The 60×1.2NA Olympus water-immersed objective focuses the excitation beam into the sample, creating a Gaussian beam waist, shown magnified on the left. The fluorescent light from the donor (Atto550) and acceptor (Atto647N) is collected by the same objective and focused by the microscope tube lens on to a 50 μm pinhole (PH), which is imaged using a 15-cm apochromat lens (AL) and a 640-nm dichroic beam splitter (BS1) into two avalanche photodiode detectors: APD1 and APD2. The counts from the APDs are acquired and analyzed by a correlator (not shown)

Next, we calibrated the confocal volume parameters, again using the free TAMRA sample, which is expected to show only diffusive behavior in the measured auto-correlation function. In this case, the auto-correlation function decays with a diffusion time constant $\tau_{diff} = r_0^2/4D_{ref}$, where r_0 is the focused beam half waist centered at the confocal volume and $D_{ref} \approx 420\ \mu m^2/s$ is the known diffusion coefficient of our reference sample [60–62]. The measured auto-correlation function for the TAMRA sample was reasonably well described by the diffusion term, with $r_0 = 328 \pm 3.3$ nm, although the data did exhibit some deviations from what is expected for three-dimensional diffusion within a perfect Gaussian volume (SI Fig. S6). We attribute these deviations to slight distortions in the shape of the confocal volume arising from less-than-ideal alignment of our confocal beam.

3.5 Matched and mismatched DNA exhibit identical diffusive dynamics

We measured the auto-correlation functions for donor-only matched (GGG/CCC_D) and mismatched (CCC/CCC_D) DNA samples. The concentration of duplex DNA in each of these samples was ~ 10 nM. Like the reference TAMRA sample, these donor-only labeled DNA samples are expected to exhibit only the diffusive dynamics, with similar correlation function decays if they have similar diffusion coefficients. Indeed, the shapes of the auto-correlation curves for the two DNA samples, after subtraction of the after-pulse component as before, were found to be identical within the noise, confirming that the two molecules have diffusion coefficients that are very close in value (SI Fig. S8). Fits to the diffusion equation, with r_0 fixed at the value obtained from the TAMRA data, yielded diffusion coefficients of $100 \pm 2.4\ \mu m^2/s$ and $97.6 \pm 2.3\ \mu m^2/s$ for the matched and mismatched samples, respectively, consistent with previous diffusion coefficient measurements for DNA oligomers of similar lengths [75–78]. Again, there were small deviations observed between the data and the fit, attributed to distortions in the Gaussian volume, as for TAMRA.

3.6 Matched DNA exhibits only diffusive dynamics while mismatched DNA also exhibits conformational dynamics

To separate diffusive dynamics from DNA conformational dynamics, we measured the donor-donor (G_{DD}) and acceptor-acceptor (G_{AA}) auto-correlation functions, acquired simultaneously on each donor–acceptor labeled matched (GGG/CCC_DA) and mismatched (CCC/CCC_DA) DNA samples. These correlation functions are expected to have contributions from both diffusion and conformational fluctuations of the DNA molecules. We followed the analysis procedure established by the Levitus and co-workers [63, 79], further described in SI Methods 1.8 and summarized in Eqs. (2)–(5), whereby the diffusive contribution drops out in the ratio G_{DD}/G_{AA} and only the conformational dynamics remains.

First, we discuss the results on the matched (GGG/CCC) DNA samples, for which all three correlation curves, (i) G_{DD} measured on donor-only sample, (ii) G_{DD} measured on donor–acceptor sample, and (iii) G_{AA} measured on donor–acceptor sample, exhibit identical shapes (SI Fig. S9a). Furthermore, the G_{DD} and G_{AA} profiles for the donor–acceptor labeled samples overlap one on top of the other, within the noise of these measurements (Fig. 4a and SI Fig. S9a), and the ratio $G_{ratio} = G_{DD}/G_{AA}$ remains close to 1 over the FCS time window (Fig. 4a; inset), indicating that contributions from DNA conformational dynamics or dye dynamics in the matched constructs are negligible. These results are reassuring and serve as an important control, since any dynamics detected on matched DNA could have had contributions from the labels fluctuating between different orientations in

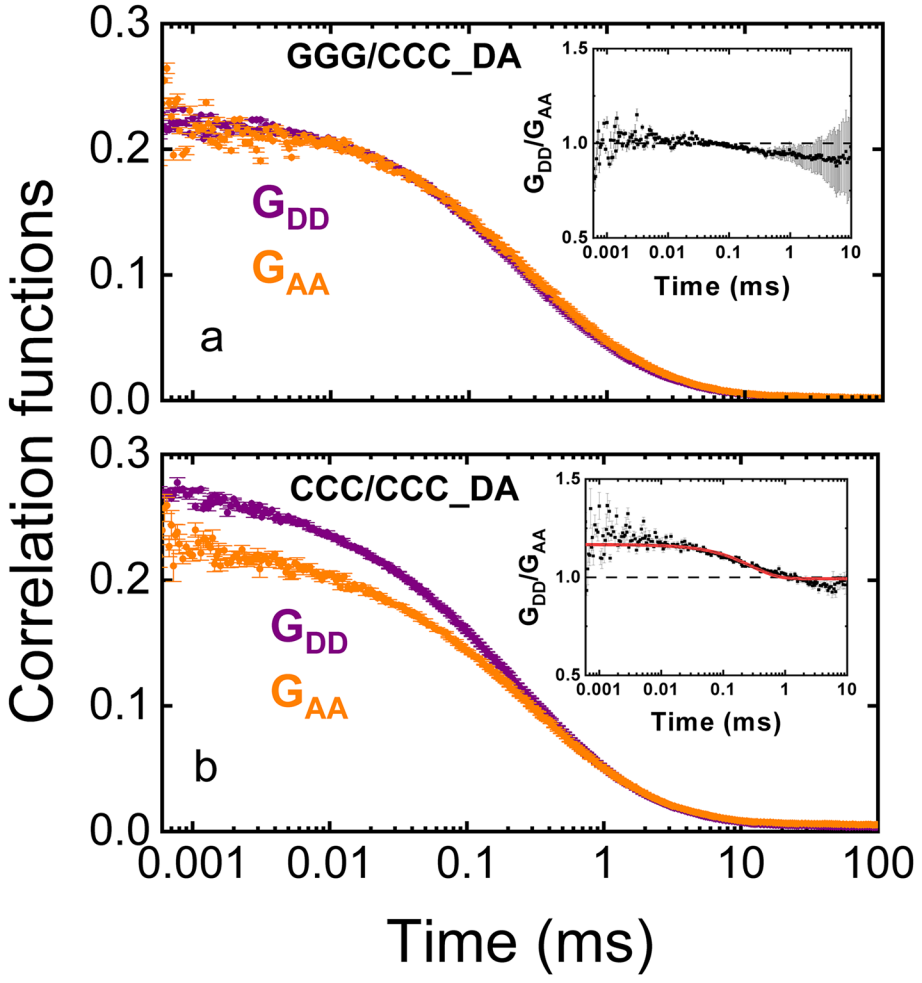

Fig. 4 Fluctuation correlation spectroscopy measurements. (**a**, **b**) The auto-correlation functions for donor (G_{DD}: purple) and acceptor (G_{AA}: orange), measured on donor–acceptor-labeled DNA samples, are plotted as a function of time for (**a**) matched (GGG/CCC_DA) and (**b**) mismatched (CCC/CCC_DA). The insets in each panel show the corresponding ratios (G_{DD}/G_{AA}) for each of the samples. The continuous red line in (**b**; inset) is a fit to Eq. (5), with $\tau_{rel} = 285 \pm 27$ µs

addition to conformational fluctuations in DNA. We note here that G_{ratio} for matched DNA exhibits what appears to be a systematic drift below 1 at long times ($> \sim 100$ µs), albeit small in comparison with the noise in the data on this timescale (Fig. 4a). The origin of this drift is not immediately evident to us, although we cannot rule out non-ideal overlap of the donor and acceptor detection volumes [80], which could account for a marginally longer molecule transit time measured in the acceptor channel, as seems to be the case for the data shown in Fig. 4a.

The correlation functions measured for the mismatched (CCC/CCC) DNA samples exhibit non-overlapping G_{DD} and G_{AA} profiles for the donor–acceptor labeled samples (Fig. 4b and SI Fig. S9b), with the two correlation functions starting out at different amplitudes at the shortest times reported, and then converging to overlapping profiles at $\gtrsim 1$ ms. The corresponding ratio

profile in this case reveals the contribution from DNA conformational dynamics and yields relaxation times for conformational fluctuations as $\tau_{rel} = 285 \pm 27$ μs (Fig. 4b; inset). These relaxation times are attributed to unwinding/bending fluctuations in these mismatched DNA.

4 Discussion

DNA damage recognition by specialized proteins is the first step in damage repair, and the repair efficiency depends critically on the ability of these proteins to pinpoint damaged DNA sites from a vast excess of undamaged sites in genomic DNA. In the NER pathway, this task falls on Rad4/XPC, which needs to recognize a wide range of bulky, helix-destabilizing lesions [81]. The protein appears to accomplish this task by sensing DNA deformability at potential lesion sites as well as pre-distorted DNA structures that are transiently presented to the protein as it scans DNA, eventually flipping out damaged nucleotides away from the protein to form a stable recognition complex [3, 34, 82–84]. This mode of recognition enables the protein to be versatile in recognizing damage of varying shapes and sizes. Previous laser T-jump studies designed to examine the dynamics of damage recognition by Rad4 used 3-bp mismatched sites as model lesions [14, 26]. These studies revealed the timescales for preliminary interrogation, occurring on ~100–500 μs, followed by Rad4-induced DNA unwinding and nucleotide flipping at the damaged sites, on ~5–10 ms. These results suggested that the preliminary interrogation step, which overlapped in time with the 1D diffusion times of Rad4 on undamaged DNA, could serve to intermittently slow down a diffusing protein [14]. Snapshots of DNA conformational distributions measured with fluorescence lifetime studies on DNA containing cytosine analog FRET probes—tC^o and tC_{nitro}—showed that specific (CCC/CCC) mismatched DNA by itself could adopt highly distorted conformations, some of which resembled the unwound/bent conformations seen in the Rad4-bound specific complex [25, 35]. The lifetime studies, however, could only provide a snapshot of the conformational distributions and not the timescales of any fluctuations. Here, we embarked on an FCS study designed to measure the conformational dynamics of DNA by itself and to examine how these dynamics in specific, mismatched DNA differed from undamaged (matched) DNA.

The FRET labels suitable for FCS measurements—Atto550 and Atto647N dyes—were placed at some distance from the mismatched site, to increase sensitivity for any bending fluctuations. While the tC^o-tC_{nitro}-probed lifetime distributions on matched DNA displayed a single B-DNA-like component, lifetime measurements with the Atto labels showed multiple components even for matched DNA. Taken together, these results indicated that multiple orientations accessible to the dyes, from their propensity to stack against duplex DNA, likely contribute to this heterogeneity. Indeed, a previous single-molecule FRET study with similar dyes attached to matched DNA oligomers reported heterogeneously distributed FRET histograms that were attributed to multiple dye orientations [72]. These studies also suggested that any dye dynamics that would average out the orientations must be slower than the ~ 1 ms binning time of the single-molecule measurements.

Despite these caveats, our measurements detected an increase in the average FRET, from ~ 0.57 in matched DNA to ~ 0.67 in DNA with a CCC/CCC mismatched site, indicating an overall larger fractional population of more distorted DNA conformations in the presence of the mismatch. Whether this increase in FRET as a result of the mismatched site reflects more bent or more unwound or some combination remains to be explored. Another FRET study with single or multiple unpaired (bulged) nucleotides established DNA bending

in the presence of such bulges [43]. Our observation that the matched and mismatched DNA exhibit nearly identical diffusive behavior despite differences in their conformational (FRET) distributions indicates that the overall translational diffusion properties of these oligomers are not very sensitive to changes in DNA shapes introduced by the CCC/CCC mismatch. The translational and rotational diffusion behavior of short DNA oligomers similar in length to the 27-mer in this study has previously been modeled by treating the DNA as rodlike objects [75–78]. One plausible explanation for the similar diffusive behavior for our matched and mismatched constructs could be that the DNA shape changes are primarily localized torsional deformations that only slightly alter the rodlike shape and dimensions, as opposed to a significant DNA bend. As demonstrated in a previous study, FRET probes tethered to DNA through flexible linkers can be responsive to DNA helicity when the probes have a tendency to stack against DNA duplexes [85]. Further experiments together with simulations are needed to ascertain the relative amplitudes of unwinding and/or bending deformations that contribute to the measured FRET changes in CCC/CCC DNA.

FCS measurements on our constructs showed no conformational dynamics in matched DNA within the time window of ~ 600 ns –10 ms, indicating that these dyes were insensitive to small-amplitude conformational fluctuations characteristic of B-DNA. Perhaps more importantly, these results demonstrated that any fluctuations in relative dye distance/orientations from dye or linker dynamics in these constructs that could alter the FRET were either too fast or too slow to interfere with DNA conformational dynamics on the FCS timescales. In contrast, we observed conformational dynamics on CCC/CCC mismatched DNA in the ~ 600 ns –1 ms time range, with a characteristic time constant of ~ 300 μs, which we attribute to DNA unwinding/bending fluctuations because of the mismatch. To our knowledge, these are the first observations of DNA unwinding/bending dynamics in mismatched DNA, distinct from single base pair opening/flipping dynamics [47, 86] or DNA looping/unlooping dynamics such as those measured in DNA cyclization studies [87–89].

Notably, these anomalous unwinding/bending fluctuations in DNA occur on timescales that overlap with the 1D diffusion times of Rad4 on undamaged DNA [10]. Thus, these studies add to the growing picture that thermally accessible distortions in lesion-containing DNA—with possibly unpaired and transiently flipped out bases—are presented to Rad4 as it sits on a given site and likely alter how Rad4 engages with that site during the search and interrogation process. Indeed, in addition to normal 1D diffusion observed in the single-molecule studies, both Rad4 and XPC also exhibit anomalous diffusion ("constrained" motion) and some population of what appear to be stalled ("immobile") proteins [10, 11]. Furthermore, the population of Rad4 molecules that exhibit constrained motion or are immobile increase in the presence of UV-damage [10]. Intriguingly, the spatial location of constrained or immobile motions seen for XPC while diffusing on undamaged DNA was found to be correlated with the presence of AT-tracts—stretches of alternating ATs—in λ-DNA [11]. Such AT-tracts have been shown to form transiently open bubbles even in the context of undamaged (matched) DNA on FCS timescales [90], lending support to the notion that significantly altered DNA structures serve as temporary trapping events for the diffusing protein [11].

Finally, we note here that an NMR and computational study on a DNA oligomer harboring a 2-bp GC/CG mismatch did not find any significant overall distortions in the DNA helical structure compared with matched DNA despite local distortions at the mismatch site [91]. That study, together with numerous others, underscores the importance of the sequence context in influencing DNA deformability and damage sensing [92–94], including a recent study that demonstrated the impact of DNA sequence on the inability of Rad4 to "open" a given site [95]. Indeed, the NER repair efficiency is known to vary widely for the diverse lesions repaired via this pathway, with the lesion structure/stereochemistry

as well as sequence context influencing the outcome [96, 97]. Further studies of intrinsic DNA flexibility and dynamics for *bonafide* NER lesions similar to the studies on model lesions reported here, and how those dynamics differ for NER-proficient versus NER-resistant lesions, would be of great value in advancing our understanding of the role that intrinsic DNA fluctuations play in the critical first step of damage sensing and recognition.

Supplementary information The online version contains supplementary material available at https://doi.org/10.1007/s10867-022-09607-x.

Acknowledgements We are deeply grateful to Marcia Levitus for her invaluable input throughout the design, development, and calibration of our home-built FCS apparatus. We also acknowledge a tremendous debt to Hans Frauenfelder, whose pioneering work on the existence of protein conformational substates opened the field of structure-dynamics-function of biomolecules.

Funding This work was supported by grants from the American Heart Association (AHA-0730254 N) to S.V.K. and from the National Science Foundation (MCB-1715649 and MCB-2107527) to A.A.

Declarations

Ethics approval Not applicable.

Informed consent Not applicable.

Conflict of interest The authors declare no competing interests.

References

1. Yang, W.: Poor base stacking at DNA lesions may initiate recognition by many repair proteins. DNA Repair (Amst) **5**, 654–666 (2006)
2. Yang, W.: Structure and mechanism for DNA lesion recognition. Cell Res. **18**, 184–197 (2008)
3. Min, J.H., Pavletich, N.P.: Recognition of DNA damage by the Rad4 nucleotide excision repair protein. Nature **449**, 570–575 (2007)
4. Ansari, A., Kuznetsov, S.V.: Dynamics and mechanism of DNA-bending proteins in binding site recognition. In: Williams, M.C., Maher, L.J. (eds.) Biophysics of DNA-Protein Interactions, pp. 107–142. Springer, New York (2010)
5. Blainey, P.C., van Oijen, A.M., Banerjee, A., Verdine, G.L., Xie, X.S.: A base-excision DNA-repair protein finds intrahelical lesion bases by fast sliding in contact with DNA. Proc. Natl. Acad. Sci. USA **103**, 5752–5757 (2006)
6. Gorman, J., Chowdhury, A., Surtees, J.A., Shimada, J., Reichman, D.R., Alani, E., Greene, E.C.: Dynamic basis for one-dimensional DNA scanning by the mismatch repair complex Msh2-Msh6. Mol. Cell **28**, 359–370 (2007)
7. Jeong, C., Cho, W.K., Song, K.M., Cook, C., Yoon, T.Y., Ban, C., Fishel, R., Lee, J.B.: MutS switches between two fundamentally distinct clamps during mismatch repair. Nat. Struct. Mol. Biol. **18**, 379–385 (2011)
8. Schonhoft, J.D., Stivers, J.T.: Timing facilitated site transfer of an enzyme on DNA. Nat. Chem. Biol. **8**, 205–210 (2012)
9. Nelson, S.R., Dunn, A.R., Kathe, S.D., Warshaw, D.M., Wallace, S.S.: Two glycosylase families diffusively scan DNA using a wedge residue to probe for and identify oxidatively damaged bases. Proc. Natl. Acad. Sci. USA **111**, E2091-2099 (2014)
10. Kong, M., Liu, L., Chen, X., Driscoll, K.I., Mao, P., Bohm, S., Kad, N.M., Watkins, S.C., Bernstein, K.A., Wyrick, J.J., Min, J.H., Van Houten, B.: Single-molecule imaging reveals that Rad4 employs a dynamic DNA damage recognition process. Mol. Cell **64**, 376–387 (2016)

11. Cheon, N.Y., Kim, H.S., Yeo, J.E., Scharer, O.D., Lee, J.Y.: Single-molecule visualization reveals the damage search mechanism for the human NER protein XPC-RAD23B. Nucleic Acids Res. **47**, 8337–8347 (2019)
12. Cho, W.K., Jeong, C., Kim, D., Chang, M., Song, K.M., Hanne, J., Ban, C., Fishel, R., Lee, J.B.: ATP alters the diffusion mechanics of MutS on mismatched DNA. Structure **20**, 1264–1274 (2012)
13. Velmurugu, Y.: Dynamics and Mechanism of DNA-bending Proteins in Binding-site Recognition. University of Illinois at Chicago, Chicago, Physics (2016)
14. Velmurugu, Y., Chen, X., Slogoff Sevilla, P., Min, J.H., Ansari, A.: Twist-open mechanism of DNA damage recognition by the Rad4/XPC nucleotide excision repair complex. Proc. Natl. Acad. Sci. USA **113**, E2296–2305 (2016)
15. Velmurugu, Y., Vivas, P., Connolly, M., Kuznetsov, S.V., Rice, P.A., Ansari, A.: Two-step interrogation then recognition of DNA binding site by Integration Host Factor: an architectural DNA-bending protein. Nucleic Acids Res. **46**, 1741–1755 (2018)
16. Slutsky, M., Mirny, L.A.: Kinetics of protein-DNA interaction: facilitated target location in sequence-dependent potential. Biophys. J. **87**, 4021–4035 (2004)
17. Zhou, H.X.: Rapid search for specific sites on DNA through conformational switch of nonspecifically bound proteins. Proc. Natl. Acad. Sci. USA **108**, 8651–8656 (2011)
18. Kalodimos, C.G., Biris, N., Bonvin, A.M., Levandoski, M.M., Guennuegues, M., Boelens, R., Kaptein, R.: Structure and flexibility adaptation in nonspecific and specific protein-DNA complexes. Science **305**, 386–389 (2004)
19. Friedman, J.I., Majumdar, A., Stivers, J.T.: Nontarget DNA binding shapes the dynamic landscape for enzymatic recognition of DNA damage. Nucleic Acids Res. **37**, 3493–3500 (2009)
20. Iwahara, J., Zweckstetter, M., Clore, G.M.: NMR structural and kinetic characterization of a homeodomain diffusing and hopping on nonspecific DNA. Proc. Natl. Acad. Sci. USA **103**, 15062–15067 (2006)
21. Obmolova, G., Ban, C., Hsieh, P., Yang, W.: Crystal structures of mismatch repair protein MutS and its complex with a substrate DNA. Nature **407**, 703–710 (2000)
22. Zheng, H., Cai, Y., Ding, S., Tang, Y., Kropachev, K., Zhou, Y., Wang, L., Wang, S., Geacintov, N.E., Zhang, Y., Broyde, S.: Base flipping free energy profiles for damaged and undamaged DNA. Chem. Res. Toxicol. **23**, 1868–1870 (2010)
23. Sharma, M., Predeus, A.V., Mukherjee, S., Feig, M.: DNA bending propensity in the presence of base mismatches: implications for DNA repair. J. Phys. Chem. B **117**, 6194–6205 (2013)
24. Panigrahi, A., Vemuri, H., Aggarwal, M., Pitta, K., Krishnan, M.: Sequence specificity, energetics and mechanism of mismatch recognition by DNA damage sensing protein Rad4/XPC. Nucleic Acids Res. **48**, 2246–2257 (2020)
25. Chakraborty, S., Steinbach, P.J., Paul, D., Mu, H., Broyde, S., Min, J.H., Ansari, A.: Enhanced spontaneous DNA twisting/bending fluctuations unveiled by fluorescence lifetime distributions promote mismatch recognition by the Rad4 nucleotide excision repair complex. Nucleic Acids Res. **46**, 1240–1255 (2018)
26. Chen, X., Velmurugu, Y., Zheng, G., Park, B., Shim, Y., Kim, Y., Liu, L., Van Houten, B., He, C., Ansari, A., Min, J.H.: Kinetic gating mechanism of DNA damage recognition by Rad4/XPC. Nat. Commun. **6**, 5849 (2015)
27. Gillet, L.C., Scharer, O.D.: Molecular mechanisms of mammalian global genome nucleotide excision repair. Chem. Rev. **106**, 253–276 (2006)
28. Puumalainen, M.R., Ruthemann, P., Min, J.H., Naegeli, H.: Xeroderma pigmentosum group C sensor: unprecedented recognition strategy and tight spatiotemporal regulation. Cell Mol. Life Sci. **73**, 547–566 (2016)
29. Riedl, T., Hanaoka, F., Egly, J.M.: The comings and goings of nucleotide excision repair factors on damaged DNA. EMBO J. **22**, 5293–5303 (2003)
30. Uchida, A., Sugasawa, K., Masutani, C., Dohmae, N., Araki, M., Yokoi, M., Ohkuma, Y., Hanaoka, F.: The carboxy-terminal domain of the XPC protein plays a crucial role in nucleotide excision repair through interactions with transcription factor IIH. DNA Repair (Amst) **1**, 449–461 (2002)
31. Yokoi, M., Masutani, C., Maekawa, T., Sugasawa, K., Ohkuma, Y., Hanaoka, F.: The xeroderma pigmentosum group C protein complex XPC-HR23B plays an important role in the recruitment of transcription factor IIH to damaged DNA. J. Biol. Chem. **275**, 9870–9875 (2000)
32. Sugasawa, K., Okamoto, T., Shimizu, Y., Masutani, C., Iwai, S., Hanaoka, F.: A multistep damage recognition mechanism for global genomic nucleotide excision repair. Genes Dev. **15**, 507–521 (2001)
33. Paul, D., Mu, H., Zhao, H., Ouerfelli, O., Jeffrey, P.D., Broyde, S., Min, J.H.: Structure and mechanism of pyrimidine-pyrimidone (6–4) photoproduct recognition by the Rad4/XPC nucleotide excision repair complex. Nucleic Acids Res. **47**, 6015–6028 (2019)

34. Buterin, T., Meyer, C., Giese, B., Naegeli, H.: DNA quality control by conformational readout on the undamaged strand of the double helix. Chem. Biol. **12**, 913–922 (2005)
35. Paul, D., Mu, H., Tavakoli, A., Dai, Q., Chen, X., Chakraborty, S., He, C., Ansari, A., Broyde, S., Min, J.H.: Tethering-facilitated DNA 'opening' and complementary roles of b-hairpin motifs in the Rad4/XPC DNA damage sensor protein. Nucleic Acids Res. **48**, 12348–12364 (2020)
36. Isaacs, R.J., Rayens, W.S., Spielmann, H.P.: Structural differences in the NOE-derived structure of G·T mismatched DNA relative to normal DNA are correlated with differences in (13)C relaxation-based internal dynamics. J. Mol. Biol. **319**, 191–207 (2002)
37. Isaacs, R.J., Spielmann, H.P.: A model for initial DNA lesion recognition by NER and MMR based on local conformational flexibility. DNA Repair (Amst) **3**, 455–464 (2004)
38. Stivers, J.T.: Site-specific DNA damage recognition by enzyme-induced base flipping. Prog. Nucleic Acid Res. Mol. Biol. **77**, 37–65 (2004)
39. Parker, J.B., Bianchet, M.A., Krosky, D.J., Friedman, J.I., Amzel, L.M., Stivers, J.T.: Enzymatic capture of an extrahelical thymine in the search for uracil in DNA. Nature **449**, 433–437 (2007)
40. Nag, N., Rao, B.J., Krishnamoorthy, G.: Altered dynamics of DNA bases adjacent to a mismatch: a cue for mismatch recognition by MutS. J. Mol. Biol. **374**, 39–53 (2007)
41. Li, Y., Lombardo, Z., Joshi, M., Hingorani, M.M., Mukerji, I.: Mismatch Recognition by Saccharomyces cerevisiae Msh2-Msh6: Role of Structure and Dynamics. Int. J. Mol. Sci. **20**, 4271 (2019)
42. Mazurek, A., Johnson, C.N., Germann, M.W., Fishel, R.: Sequence context effect for hMSH2-hMSH6 mismatch-dependent activation. Proc. Natl. Acad. Sci. USA **106**, 4177–4182 (2009)
43. Wozniak, A.K., Schroder, G.F., Grubmuller, H., Seidel, C.A., Oesterhelt, F.: Single-molecule FRET measures bends and kinks in DNA. Proc. Natl. Acad. Sci. USA **105**, 18337–18342 (2008)
44. Patel, D.J., Kozlowski, S.A., Ikuta, S., Itakura, K.: Dynamics of DNA duplexes containing internal G.T, G.A, A.C, and T.C pairs: hydrogen exchange at and adjacent to mismatch sites. Fed. Proc. **43**, 2663–2670 (1984)
45. Pardi, A., Morden, K.M., Patel, D.J., Tinoco, Jr., I.: Kinetics for exchange of imino protons in the d(C-G-C-G-A-A-T-T-C-G-C-G) double helix and in two similar helices that contain a G·T base pair, d(C-G-T-G-A-A-T-T-C-G-C-G), and an extra adenine, d(C-G-C-A-G-A-A-T-T-C-G-C-G). Biochemistry **21**, 6567–6574 (1982)
46. Patel, D.J., Pardi, A., Itakura, K.: DNA conformation, dynamics, and interactions in solution. Science **216**, 581–590 (1982)
47. Moe, J.G., Russu, I.M.: Kinetics and energetics of base-pair opening in 5'-d(CGCGAATTCGCG)-3' and a substituted dodecamer containing G.T mismatches. Biochemistry **31**, 8421–8428 (1992)
48. Bhattacharya, P.K., Cha, J., Barton, J.K.: 1H NMR determination of base-pair lifetimes in oligonucleotides containing single base mismatches. Nucleic Acids Res. **30**, 4740–4750 (2002)
49. Kim, J.K., Choi, B.S.: The solution structure of DNA duplex-decamer containing the (6–4) photoproduct of thymidylyl(3'–>5')thymidine by NMR and relaxation matrix refinement. Eur. J. Biochem. **228**, 849–854 (1995)
50. Kim, J.K., Patel, D., Choi, B.S.: Contrasting structural impacts induced by cis-syn cyclobutane dimer and (6–4) adduct in DNA duplex decamers: implication in mutagenesis and repair activity. Photochem. Photobiol. **62**, 44–50 (1995)
51. Kemmink, J., Boelens, R., Koning, T.M., Kaptein, R., van der Marel, G.A., van Boom, J.H.: Conformational changes in the oligonucleotide duplex d(GCGTTGCG) x d(CGCAACGC) induced by formation of a cis-syn thymine dimer. A two-dimensional NMR study. Eur. J. Biochem. **162**, 37–43 (1987)
52. Wang, C.I., Taylor, J.S.: Site-specific effect of thymine dimer formation on dAn.dTn tract bending and its biological implications. Proc. Natl. Acad. Sci. USA **88**, 9072–9076 (1991)
53. Borjesson, K., Preus, S., El-Sagheer, A.H., Brown, T., Albinsson, B., Wilhelmsson, L.M.: Nucleic acid base analog FRET-pair facilitating detailed structural measurements in nucleic acid containing systems. J. Am. Chem. Soc. **131**, 4288–4293 (2009)
54. Preus, S., Borjesson, K., Kilsa, K., Albinsson, B., Wilhelmsson, L.M.: Characterization of nucleobase analogue FRET acceptor tCnitro. J. Phys. Chem. B. **114**, 1050–1056 (2010)
55. Preus, S., Wilhelmsson, L.M.: Advances in quantitative FRET-based methods for studying nucleic acids. ChemBioChem **13**, 1990–2001 (2012)
56. Dumat, B., Larsen, A.F., Wilhelmsson, L.M.: Studying Z-DNA and B- to Z-DNA transitions using a cytosine analogue FRET-pair. Nucleic Acids Res. **44**, e101 (2016)
57. O'Connor, D.V.: Time-correlated Single Photon Counting. Academic Press, London (1984)
58. Steinbach, P.J., Ionescu, R., Matthews, C.R.: Analysis of kinetics using a hybrid maximum-entropy/nonlinear-least-squares method: application to protein folding. Biophys. J. **82**, 2244–2255 (2002)

59. Steinbach, P.J.: Filtering artifacts from lifetime distributions when maximizing entropy using a bootstrapped model. Anal. Biochem. **427**, 102–105 (2012)
60. Petrasek, Z., Schwille, P.: Precise measurement of diffusion coefficients using scanning fluorescence correlation spectroscopy. Biophys. J. **94**, 1437–1448 (2008)
61. Gendron, P.O., Avaltroni, F., Wilkinson, K.J.: Diffusion coefficients of several rhodamine derivatives as determined by pulsed field gradient-nuclear magnetic resonance and fluorescence correlation spectroscopy. J. Fluoresc. **18**, 1093–1101 (2008)
62. Ranjit, S., Levitus, M.: Probing the interaction between fluorophores and DNA nucleotides by fluorescence correlation spectroscopy and fluorescence quenching. Photochem. Photobiol. **88**, 782–791 (2012)
63. Torres, T., Levitus, M.: Measuring conformational dynamics: a new FCS-FRET approach. J. Phys. Chem. B. **111**, 7392–7400 (2007)
64. Sandin, P., Borjesson, K., Li, H., Martensson, J., Brown, T., Wilhelmsson, L.M., Albinsson, B.: Characterization and use of an unprecedentedly bright and structurally non-perturbing fluorescent DNA base analogue. Nucleic Acids Res. **36**, 157–167 (2008)
65. Gauer, J.W., LeBlanc, S., Hao, P., Qiu, R., Case, B.C., Sakato, M., Hingorani, M.M., Erie, D.A., Weninger, K.R.: Single-molecule FRET to measure conformational dynamics of DNA mismatch repair proteins. Methods Enzymol. **581**, 285–315 (2016)
66. Ha, T.: Single-molecule fluorescence resonance energy transfer. Methods **25**, 78–86 (2001)
67. Hellenkamp, B., Schmid, S., Doroshenko, O., Opanasyuk, O., Kuhnemuth, R., Rezaei Adariani, S., Ambrose, B., Aznauryan, M., Barth, A., Birkedal, V., Bowen, M.E., Chen, H., Cordes, T., Eilert, T., Fijen, C., Gebhardt, C., Gotz, M., Gouridis, G., Gratton, E., Ha, T., Hao, P., Hanke, C.A., Hartmann, A., Hendrix, J., Hildebrandt, L.L., Hirschfeld, V., Hohlbein, J., Hua, B., Hubner, C.G., Kallis, E., Kapanidis, A.N., Kim, J.Y., Krainer, G., Lamb, D.C., Lee, N.K., Lemke, E.A., Levesque, B., Levitus, M., McCann, J.J., Naredi-Rainer, N., Nettels, D., Ngo, T., Qiu, R., Robb, N.C., Rocker, C., Sanabria, H., Schlierf, M., Schroder, T., Schuler, B., Seidel, H., Streit, L., Thurn, J., Tinnefeld, P., Tyagi, S., Vandenberk, N., Vera, A.M., Weninger, K.R., Wunsch, B., Yanez-Orozco, I.S., Michaelis, J., Seidel, C.A.M., Craggs, T.D., Hugel, T.: Precision and accuracy of single-molecule FRET measurements-a multi-laboratory benchmark study. Nat. Methods **15**, 669–676 (2018)
68. Fuller, J.R., Rice, P.A.: Target DNA bending by the Mu transpososome promotes careful transposition and prevents its reversal. eLife **6**, e21777 (2017)
69. Schuler, B., Lipman, E.A., Eaton, W.A.: Probing the free-energy surface for protein folding with single-molecule fluorescence spectroscopy. Nature **419**, 743–747 (2002)
70. Kupstat, A., Ritschel, T., Kumke, M.U.: Oxazine dye-conjugated dna oligonucleotides: Forster resonance energy transfer in view of molecular dye-DNA interactions. Bioconjug. Chem. **22**, 2546–2557 (2011)
71. Hartmann, A., Krainer, G., Schlierf, M.: Different fluorophore labeling strategies and designs affect millisecond kinetics of DNA hairpins. Molecules **19**, 13735–13754 (2014)
72. Vandenberk, N., Barth, A., Borrenberghs, D., Hofkens, J., Hendrix, J.: Evaluation of blue and far-red dye pairs in single-molecule forster resonance energy transfer experiments. J. Phys. Chem. B **122**, 4249–4266 (2018)
73. Ishii, K., Tahara, T.: Correction of the afterpulsing effect in fluorescence correlation spectroscopy using time symmetry analysis. Opt. Express **23**, 32387–32400 (2015)
74. Slenders, E., Castello, M., Buttafava, M., Villa, F., Tosi, A., Lanzano, L., Koho, S.V., Vicidomini, G.: Confocal-based fluorescence fluctuation spectroscopy with a SPAD array detector. Light Sci. Appl. **10**, 31 (2021)
75. Eimer, W., Pecora, R.: Rotational and translational diffusion of short rodlike molecules in solution: Oligonucleotides. J. Chem. Phys. **94**, 2324–2329 (1991)
76. Bonifacio, G.F., Brown, T., Conn, G.L., Lane, A.N.: Comparison of the electrophoretic and hydrodynamic properties of DNA and RNA oligonucleotide duplexes. Biophys. J. **73**, 1532–1538 (1997)
77. Stellwagen, N.C., Magnusdottir, S., Gelfi, C., Righetti, P.G.: Measuring the translational diffusion coefficients of small DNA molecules by capillary electrophoresis. Biopolymers **58**, 390–397 (2001)
78. Stellwagen, E., Stellwagen, N.C.: Determining the electrophoretic mobility and translational diffusion coefficients of DNA molecules in free solution. Electrophoresis **23**, 2794–2803 (2002)
79. Li, G., Levitus, M., Bustamante, C., Widom, J.: Rapid spontaneous accessibility of nucleosomal DNA. Nat. Struct. Mol. Biol. **12**, 46–53 (2005)
80. Kudryavtsev, V., Sikor, M., Kalinin, S., Mokranjac, D., Seidel, C.A., Lamb, D.C.: Combining MFD and PIE for accurate single-pair Forster resonance energy transfer measurements. ChemPhysChem **13**, 1060–1078 (2012)

81. Mu, H., Geacintov, N.E., Broyde, S., Yeo, J.E., Scharer, O.D.: Molecular basis for damage recognition and verification by XPC-RAD23B and TFIIH in nucleotide excision repair. DNA Repair (Amst) **71**, 33–42 (2018)
82. Gunz, D., Hess, M.T., Naegeli, H.: Recognition of DNA adducts by human nucleotide excision repair. Evidence for a thermodynamic probing mechanism. J. Biol. Chem. **271**, 25089–25098 (1996)
83. Geacintov, N.E., Broyde, S., Buterin, T., Naegeli, H., Wu, M., Yan, S., Patel, D.J.: Thermodynamic and structural factors in the removal of bulky DNA adducts by the nucleotide excision repair machinery. Biopolymers **65**, 202–210 (2002)
84. Maillard, O., Camenisch, U., Clement, F.C., Blagoev, K.B., Naegeli, H.: DNA repair triggered by sensors of helical dynamics. Trends Biochem. Sci. **32**, 494–499 (2007)
85. Iqbal, A., Arslan, S., Okumus, B., Wilson, T.J., Giraud, G., Norman, D.G., Ha, T., Lilley, D.M.: Orientation dependence in fluorescent energy transfer between Cy3 and Cy5 terminally attached to double-stranded nucleic acids. Proc. Natl. Acad. Sci. USA **105**, 11176–11181 (2008)
86. Yin, Y., Yang, L., Zheng, G., Gu, C., Yi, C., He, C., Gao, Y.Q., Zhao, X.S.: Dynamics of spontaneous flipping of a mismatched base in DNA duplex. Proc. Natl. Acad. Sci. USA **111**, 8043–8048 (2014)
87. Peters, J.P., 3rd., Maher, L.J.: DNA curvature and flexibility in vitro and in vivo. Q. Rev. Biophys. **43**, 23–63 (2010)
88. Vafabakhsh, R., Ha, T.: Extreme bendability of DNA less than 100 base pairs long revealed by single-molecule cyclization. Science **337**, 1097–1101 (2012)
89. Yeou, S., Lee, N.K.: Single-molecule methods for investigating the double-stranded DNA bendability. Mol. Cells **45**, 33–40 (2022)
90. Altan-Bonnet, G., Libchaber, A., Krichevsky, O.: Bubble dynamics in double-stranded DNA. Phys. Rev. Lett. **90**, 138101 (2003)
91. Ghosh, A., Kar, R.K., Krishnamoorthy, J., Chatterjee, S., Bhunia, A.: Double GC:GC mismatch in dsDNA enhances local dynamics retaining the DNA footprint: a high-resolution NMR study. ChemMedChem **9**, 2059–2064 (2014)
92. Cai, Y., Patel, D.J., Geacintov, N.E., Broyde, S.: Differential nucleotide excision repair susceptibility of bulky DNA adducts in different sequence contexts: hierarchies of recognition signals. J. Mol. Biol. **385**, 30–44 (2009)
93. Kropachev, K., Kolbanovskii, M., Cai, Y., Rodriguez, F., Kolbanovskii, A., Liu, Y., Zhang, L., Amin, S., Patel, D., Broyde, S., Geacintov, N.E.: The sequence dependence of human nucleotide excision repair efficiencies of benzo[a]pyrene-derived DNA lesions: insights into the structural factors that favor dual incisions. J. Mol. Biol. **386**, 1193–1203 (2009)
94. Cai, Y., Patel, D.J., Geacintov, N.E., Broyde, S.: Dynamics of a benzo[a]pyrene-derived guanine DNA lesion in TGT and CGC sequence contexts: enhanced mobility in TGT explains conformational heterogeneity, flexible bending, and greater susceptibility to nucleotide excision repair. J. Mol. Biol. **374**, 292–305 (2007)
95. Paul, D., Mu, H., Tavakoli, A., Dai, Q., Chakraborty, S., He, C., Ansari, A., Broyde, S., Min, J.H.: Impact of DNA sequences on DNA 'opening' by the Rad4/XPC nucleotide excision repair complex. DNA Repair (Amst) **107**, 103194 (2021)
96. Kropachev, K., Kolbanovskiy, M., Liu, Z., Cai, Y., Zhang, L., Schwaid, A.G., Kolbanovskiy, A., Ding, S., Amin, S., Broyde, S., Geacintov, N.E.: Adenine-DNA adducts derived from the highly tumorigenic Dibenzo[a, l]pyrene are resistant to nucleotide excision repair while guanine adducts are not. Chem. Res. Toxicol. **26**, 783–793 (2013)
97. Mu, H., Zhang, Y., Geacintov, N.E., Broyde, S.: Lesion Sensing during Initial Binding by Yeast XPC/Rad4: Toward Predicting Resistance to Nucleotide Excision Repair. Chem. Res. Toxicol. **31**, 1260–1268 (2018)